Published in final edited form as:
Mol Cell. 2009 April 24; 34(2): 155–167. doi:10.1016/j.molcel.2009.02.032.

An Alpha Motif at Tas3 C Terminus Mediates RITS *cis* Spreading and Promotes Heterochromatic Gene Silencing

Haitao Li[1,4], **Mohammad R. Motamedi**[2,4], **Calvin K. Yip**[2], **Zhanxin Wang**[1], **Thomas Walz**[2,3], **Dinshaw J. Patel**[1,*], and **Danesh Moazed**[2,3,*]

[1]Structural Biology Program, Memorial Sloan-Kettering Cancer Center, New York, NY 10065, USA

[2]Department of Cell Biology, Harvard Medical School, Boston, MA 02115, USA

[3]Howard Hughes Medical Institute, Harvard Medical School, Boston, MA 02115, USA

SUMMARY

RNA interference (RNAi) plays a pivotal role in the formation of heterochromatin at the fission yeast centromeres. The RNA-induced transcriptional silencing (RITS) complex, composed of heterochromatic small interfering RNAs (siRNAs), the siRNA-binding protein Ago1, the chromodomain protein Chp1, and the Ago1/Chp1-interacting protein Tas3, provides a physical tether between the RNAi and heterochromatin assembly pathways. Here, we report the structural and functional characterization of a C-terminal Tas3 α-helical motif (TAM), which self-associates into a helical polymer and is required for *cis* spreading of RITS in centromeric DNA regions. Site-directed mutations of key residues within the hydrophobic monomer-monomer interface disrupt Tas3-TAM polymeric self-association in vitro and result in loss of gene silencing, spreading of RITS, and a dramatic reduction in centromeric siRNAs in vivo. These results demonstrate that, in addition to the chromodomain of Chp1 and siRNA-loaded Ago1, Tas3 self-association is required for RITS spreading and efficient heterochromatic gene silencing at centromeric repeat regions.

INTRODUCTION

In eukaryotes, the formation of silent chromatin or heterochromatin is critical for a variety of cellular processes including global regulation of gene expression, centromere and telomere function, dosage compensation, and the maintenance of genomic stability. Posttranslational modifications of histone tails, catalyzed by histone-modifying proteins, organize chromosomes into functionally distinct domains (Grewal and Moazed, 2003; Richards and Elgin, 2002). A critical modification involved in the demarcation of heterochromatin is the methylation of histone H3 at lysine 9 (H3K9me) by conserved KMT1 histone methyltransferases (Clr4 in fission yeast and Suv39h in humans) (Rea et al., 2000). H3K9me is the binding substrate for the conserved HP1 family of chromosomal proteins (Jacobs et al., 2001; Lachner et al., 2001), which are a major constituent of eukaryotic heterochromatin. The spreading of HP1-

*Correspondence: pateld@mskcc.org (D.J.P.), danesh@hms.harvard.edu (D.M.).
[4]These authors contributed equally to this work

ACCESSION NUMBERS

Coordinates have been deposited in the Protein Data Bank with accession codes 3D1B for tetragonal and 3D1D for hexagonal Tas3 C-terminal domain structures.

SUPPLEMENTAL DATA

The Supplemental Data include six figures, two tables, and Supplemental Experimental Procedures and can be found with this article online at http://www.cell.com/molecular-cell/supplemental/S1097-2765(09)00148-8.

based heterochromatin in fission yeast and other eukaryotes has been proposed to involve iterative cycles of histone H3K9 methylation by the KMT1 methyltransferase, coupled to subsequent recruitment of HP1 by a mechanism that may involve HP1 oligomerization (Bannister et al., 2001; Grewal and Moazed, 2003; Nakayama et al., 2001). However, recent studies suggest that the spreading of H3K9 methylation in fission yeast centromeric DNA regions occurs by an RNA-dependent mechanism that is largely or entirely independent of HP1 (Motamedi et al., 2008; Sadaie et al., 2004; Verdel et al., 2004; Volpe et al., 2002).

In the three chromosomes of the fission yeast *Schizosaccharomyces pombe*, large tracks of heterochromatin are found at the telomeres, the mating-type and ribosomal DNA loci, and the pericentromeric innermost (*imr)* and outer (*otr*) repeats (Ekwall, 2004; White and Allshire, 2008). The central core region of centromeres (*cnt*), symmetrically flanked by *imr* and *otr* repeats, is excluded from heterochromatin-specific factors and modifications by the presence of three transfer RNA (tRNA) genes in *imr* acting as boundary elements that limit the spreading of heterochromatin (Scott et al., 2006). Furthermore, noncoding centromeric transcripts, which appear to be an integral component of heterochromatin (Motamedi et al., 2004), have been mapped to the *dg* and *dh* DNA element within *otr* (Volpe et al., 2002; Djupedal et al., 2005).

The fission yeast RNA interference (RNAi) proteins Dicer ribonuclease (Dcr1), RNA-dependent RNA polymerase (Rdp1), and Argonaute (Ago1) are required for the establishment and maintenance of pericentromeric heterochromatin. Deletion of any of these genes results in loss of transcriptional and cotranscriptional silencing of centromeric reporter genes, decrease in Clr4-dependent H3K9 methylation and Swi6 localization at native centromeric DNA, loss of small interfering RNAs (siRNAs), and accumulation of noncoding centromeric transcripts (Volpe et al., 2002; Verdel et al., 2004). Ago1- and Rdp1-bearing complexes have been purified (called RNA-induced transcriptional silencing [RITS] and RNA-dependent RNA polymerase complex [RDRC], respectively) and were shown to interact with each other and with centromeric transcripts in an H3K9me- and siRNA-dependent manner (Motamedi et al., 2004; Verdel et al., 2004). Additionally, Dcr1 physically interacts with RDRC, and the Dcr1 ribonuclease and RDRC double-stranded RNA (dsRNA) synthesis activities are coupled in vitro (Colmenares et al., 2007). Artificial tethering of a RITS component, Tas3, to the RNA of a euchromatic gene leads to gene silencing, H3K9 methylation of the gene, Swi6 recruitment, and siRNA generation, demonstrating that recruitment of RITS to nascent transcripts can lead to heterochromatin-specific modification of the target gene (Buhler et al., 2006). Interestingly, this silencing occurs without a concomitant decrease in the transcription rate of the euchromatic gene, suggesting that a cotranscriptional degradation pathway also plays a critical role in regulating the steady-state levels of some transcripts originating from heterochromatin. Collectively, these results have led to a proposal in which chromatin modifications (e.g., H3K9me) and noncoding centromeric transcripts recruit RNAi and heterochromatin proteins to mediate gene silencing by two pathways: (1) by limiting access of RNA polymerase II transcription machinery and (2) by degrading chromatin-bound transcripts during or after synthesis (Buhler et al., 2007; Motamedi et al., 2008).

The RITS complex physically links the RNAi pathway to heterochromatin assembly. It is composed of the siRNA-binding protein Ago1, a chromodomain protein Chp1, and an Ago1/Chp1-interacting protein Tas3 (Verdel et al., 2004). RITS-associated siRNAs map to all heterochromatic loci (Cam et al., 2005; Buhler et al., 2008), and its Chp1 chromodomain subunit binds H3K9-methylated nucleosomes (Partridge et al., 2002). RITS localizes to heterochromatin in an H3K9me- and siRNA-dependent manner, and is thus tethered to heterochromatin via siRNA base-pairing interactions with heterochromatic transcripts and Chp1 binding to H3K9me. Like the other components of RITS, Tas3 is required for RNAi-dependent silencing at centromeres (Verdel et al., 2004). It links Chp1 and Ago1 and is capable of forming subcomplexes with Ago1 and Chp1 independently of the other proteins

(DeBeauchamp et al., 2008; Partridge et al., 2007; Petrie et al., 2005). Tas3 and other Ago-interacting proteins contain the evolutionary conserved GW or Ago hook motif, which mediates binding to the Argonaute PIWI domain (Partridge et al., 2007; Till et al., 2007).

The methylation of H3K9 at centromeres is mediated by two distinct mechanisms that make unique contributions to its nucleation and spreading. First, an RNAi-independent pathway mediates low levels of H3K9me within *imr* and the *dg* and *dh* repeats in *otr*. Second, an RNAi-based mechanism boosts this methylation and is required for its spreading to reporter genes that are inserted within either *imr* or *otr* (Volpe et al., 2002; Verdel et al., 2004; Sadaie et al., 2004). Therefore, in the absence of RNAi, H3K9me fails to spread into sequences associated with reporter genes and silencing of centromeric reporter genes is abrogated. The nascent transcript model, in which the RITS and RNAi complexes associate with nascent noncoding centromeric RNAs (Motamedi et al., 2004), provides an explanation for RNAi-dependent spreading of H3K9 methylation to transcribed centromeric regions. However, how RITS spreads to regions that are apparently not transcribed has remained unclear. Here, we present the structure of the C-terminal ~120 amino acids of Tas3, henceforth referred to as Tas3-TAM (Tas3 α-helical motif), and find that it forms an all α-helical structure capable of polymeric self-association in vitro. Amino acid substitutions that disrupt Tas3-TAM self-association also cause a loss of silencing of a reporter gene inserted at *imr*, but only show a slight defect in silencing at *otr*, suggesting that RITS spreading to reporter genes at *imr* requires Tas3 self-association. Surprisingly, chromatin immunoprecipitation (ChIP) experiments reveal that in *tas3-TAM* mutants H3K9me levels are unaffected at the native *imr* sequences, but RITS spreading to *imr* is completely abolished. These findings reveal a critical role for Tas3-mediated RITS spreading, downstream of H3K9 methylation, in silencing of centromeric transgenes.

RESULTS

Structure of the Tas3 C-Terminal Domain

In an attempt to explore the domain architecture of Tas3, we identified a globular domain at the Tas3 C terminus by hydrophobic cluster analysis (Gaboriaud et al., 1987)(Figure 1A and see Figure S1 available online), which shares no obvious sequence homology with other known modules. To gain insights into the potential function of this C-terminal domain, we overexpressed and purified two constructs from the Tas3 C terminus for structural studies, namely Te (426−549) and Te1 (426−545), and solved the crystal structures of Te1 in two crystal forms at 1.7 Å and 2.6 Å, respectively (data collection and refinement statistics are listed in Table 1). It is worth noting that though similar tetragonal crystals could be obtained for both Te and Te1 constructs, deletion of four residues from the C terminus significantly improves the diffraction quality of the crystal from ~3.6 Å to 1.7 Å, which is likely due to the mobility of the last four residues and their interference with periodic crystal packing.

Structural determination revealed an all-α-helical motif at the Tas3 C terminus, which spans residue 434−544 and is composed of seven α helices that fold into an ellipsoid-shaped compact module (Figures 1B and 1C). In the solved structures from both crystal forms, approximately eight to ten residues from the N terminus and one residue from the C terminus were not modeled due to high flexibility and lack of sufficient density. The Tas3 C-terminal alpha motif (designated TAM) can be further divided into two subdomains, with each containing a triangular three-helix up-and-down bundle (Figure 1C). The first subdomain composed of helices α1 to α3 and the second subdomain comprised of helices α4 to α6 are connected by a 13-residue loop, which notably caps subdomain 2 from the top, holding the two subdomains together (Figures 1C and S2A). There are extensive hydrophobic interactions between the two subdomains with a buried surface of 618 $Å^2$, which significantly stabilizes the compact fold of the TAM domain (Figure S2A).

To identify the similarity of TAM with other known structures in the PDB database, we performed structure-based domain alignment through secondary structure matching (Krissinel and Henrick, 2004). No reasonable hit was found when the TAM monomer was used for alignment (Figure S3A). When individual subdomains were used as the query, it turned out that each subdomain shares similar immunoglobulin folds with some three-helical bundle domains, such as the ubiquitin ligase UBA domain, IgG-binding protein A B domain, and the phosphoprotein XD domain, a characteristic property of which is to mediate protein-protein interactions via helix bundle formation in two modes (Figures S3B–S3D). However, due to lack of key conserved residues and low sequence identity, it is very likely that such similarity is restricted to the protein fold level.

TAM Domain Forms a Helical Polymer in the Crystal

Gel filtration analysis indicated that the TAM-containing constructs form a trimer in solution (Figure 2A). However, in the solved crystal structures, no closed trimer could be identified, although there are three and six molecules in one asymmetric unit of the tetragonal and the hexagonal crystal forms, respectively (Figure S4A). The Tas3-TAM domain forms a right-handed helical polymer in the crystal in which TAM monomers are arranged in head-to-tail fashion with approximately 12_5 screw symmetry (Figures 1D and S4B). The helical polymer is quite compact, with a helix diameter of ~50 Å and a rise of ~14 Å per monomer, which corresponds to about one twelfth of the length of the unit cell C axis in both crystal forms (Figures 1D and S4B). There is no visible central hole in the helical polymer, and both the N and C termini point outward from the polymeric helix (Figures 1D and S4B), thereby being positioned to accommodate the rest of the Tas3 protein and likely the RITS complex. The single peak observed for the Tas3-TAM domain during gel filtration suggests that it forms a relatively stable trimeric intermediate, which might function as a building block for longer polymer formation.

The major polymerization interface is formed between helices a4 and a5 of one monomer and helices α2 and α3 of the adjacent one (Figures 1C and 1E). These helices form a four-helix bundle, with a buried area of ~553 $Å^2$, which corresponds to about 9% of the monomer surface area. The interface has a hydrophobic core that is surrounded by a network of hydrogen bonds and salt bridges (Figure S2B). The hydrophobic interactions are contributed by residues L495, L499, L502, L505, and Y520 from one monomer and V462, L470, I471, and L479 from another, with association specificity particularly facilitated by considerable shape complementarity (Figures 1E and S2B). Among those hydrophobic residues, I471, L479, and L502 localize to the center of the hydrophobic core and are predicted to be critical for TAM helical polymer formation (Figure 1E). It is worth noting that there exists a surface channel between α4 and α6 in the exposed surface of TAM monomer (Figure 1C) as well as TAM polymer (Figure 1D). Whether such a surface channel could act as a functional binding pocket remains to be explored.

Beyond the major polymerization interface discussed above, the long linker connecting the two subdomains also participates in the polymerization through polar interactions (hydrogen bonding and salt bridge) with the bottom region of the monomers at +2 and +3 positions (Figure S2C). Such a linker loop is partially buried upon TAM polymerization. Altogether, about 30% surface area of the monomer is buried on polymer formation. Furthermore, surface electrostatic potential analysis uncovered the dipole nature of the TAM polymer in which one end of the polymer is mostly negatively charged and the other largely positively charged (Figures 1D and S4C). Such a unique dipole charge distribution could act as a driving force to prompt TAM polymerization in solution. TAM polymerization neutralizes the opposing electrostatic charges at the two polymer poles and leaves the exposed surface mainly negatively charged along the polymer (Figures 1D and S4C).

TAM-Mediated Homotypic Polymerization in Solution

We next performed a series of biochemical and biophysical experiments in combination with site-directed mutagenesis to explore the Tas3 self-association of Tas3 in solution.

We introduced L to E mutations at positions 479 and 502, constituting the hydrophobic core of the major polymerization interface in the Te (426−549) construct, and were able to overexpress the mutant protein in *Escherichia coli* and purify it to high homogeneity. Circular dichroism spectra analysis suggested that the double mutation did not affect the all-α-helical folding of TAM domain (Figure S5). We also tried to express Te constructs carrying single point mutations I471E, L479E, and L502E, but their expression levels were too low to yield a reasonable amount of recombinant proteins for further in vitro assays.

In gel-filtration analysis, the peak of Te (L479E/L502E) double mutant (TeDM) shifted toward a lower oligomeric state, likely to its monomeric form, with an apparent molecular weight of ~15 kD (Figure 2A). This suggests that TAM domain self-association is disrupted by the two mutations and confirms that the polymerization interface identified in the crystal structure mediates TAM self-association in solution.

We also monitored the 2D ^{1}H, ^{15}N-heteronuclear single quantum coherence (HSQC) nuclear magnetic resonance (NMR) spectra of Te and TeDM samples. As shown in Figure 2B, the wild-type Te gives broad and overlapping peaks, indicating an aggregation state of the sample in solution, with the broadened characteristics remaining unchanged on lowering the protein concentration to 50 μM (Figure S6). In contrast, the TeDM sample yielded much better dispersed HSQC spectra even at a protein concentration of 750 μM, suggesting that the point mutations disrupt Te aggregation. Notably, comparison of the 2D NMR spectra of wild-type and mutant Te revealed widely distributed cross peaks of similar profile, which displayed essentially the same chemical shifts, especially at the ^{1}H downfield region (Figure 2B, arrows). This suggests that the wild-type and mutant Te proteins are similarly folded in solution and the broadened HSQC signals of the wild-type protein likely results from the increased molecular weight caused by TAM oligomerization.

Crosslinking assays were adopted to further verify the self-association of Te in solution. In a temporal profile crosslinking assay, the Te sample gave clear visible gradient bands up to an octamer in a denaturing polyacrylamide gel within a short reaction time of 15 s (Figure 2C, top left). Following the increment of reaction time, higher polymer gradient bands were observed concomitant with the consumption of lower oligomeric sample (Figure 2C, top left). As expected, the TeDM sample displayed greatly impaired self-association and yielded a similar crosslinking profile to that of a monomeric protein (RNase A) control even after 45 min of reaction (Figure 2C, top right). Similar crosslinking assays were also performed on a longer Tas3 C-terminal construct (380−549), namely Th, and the full-length Tas3. After crosslinking, both samples yielded clear gradient bands with a substantial portion of high molecular weight polymer accumulating on the top of the 4%–12% SDS-polyacrylamide gradient gels (Figure 2C, lower panels). These results revealed that the extra N-terminal part of Tas3 does not interfere with, and may even enhance, the TAM domain-mediated Tas3 self-association.

To further confirm the Tas3 polymer formation, we examined the TAM-containing Tas3 samples by negative stain electron microscopy. Although we were unable to detect polymers of the crystallized Te (426−549) sample, ordered long filaments with a width of around 20 nm and lengths of up to several micrometers were consistently observed for the slightly longer Th (380−549) construct (Figure 2D, left). Notably, the single mutation (L479E) completely abrogates Th filament formation (Figure 2D, right). This clearly demonstrates the polymerization potential of the TAM domain and supports a role for the interface identified in

the X-ray structure in this polymerization. The capability of Th, but not of the Te fragment, to form long filaments supports a role of additional residues in the N-terminal portion of Th in prompting long TAM polymer formation and potentially stabilizing these higher ordered oligomeric forms. This is consistent with the crosslinking results in which much larger crosslinked species were observed for the Th fragment even after a 15 s reaction (Figure 2C, bottom left). The extra N-terminal fragment (380−425) of Th contains a patch of basic residues and lacks a clear hydrophobic cluster (Figure S1). Given the negatively charged surface of TAM polymer (Figures 1D and S4C), this extra 46-residue fragment might play a role in interlocking TAM monomers via electrostatic interactions, thereby facilitating long filament formation of Th. In summary, the above data support polymeric self-association of Tas3 in solution.

Tas3-TAM Polymerization Mutants Display Loss of Silencing Specifically at the Centromeric *imr* Repeats

Because the Tas3-TAM domain polymerizes in vitro, we hypothesized that this domain may be involved in RITS spreading from heterochromatin nucleation centers in vivo. To test this, we introduced the TAM hydrophobic core substitutions (I471E, L479E, and L502E; see Figure 1C) into the genomic *tas3-TAP* allele in strains with *cen::ura4*$^+$ reporter inserted at *imr1R* or the *dg* repeat of *otr1R* (Figure 3A). In contrast to *tas3Δ* cells in which *ura4*$^+$ silencing is lost at both *imr1R* and *otr1R* (Verdel et al., 2004), cells carrying the wild-type *tas3-TAP* allele efficiently silenced *imr1R::ura4*$^+$ or *otr1R::ura4*$^+$, as determined by growth on media containing 5-fluoro-oratic acid, a drug toxic to *ura4*$^+$ cells, indicating that the *tas3-TAP* allele was fully functional (Figure 3B). If the Tas3-TAM domain is required for RITS spreading from *otr* to *imr*, we predict that silencing of the *imr1R::ura4*$^+$ reporter should be lost in the *tas3-TAM* mutant cells compared to the wild-type cells. Consistent with this expectation, we observed a loss of silencing of the *imr1R::ura4*$^+$ reporter for *tas3ΔTAM* and each of the point mutations (Figure 3B, top), but relatively smaller silencing defects for the *otr1R::ura4*$^+$ reporter (Figure 3B, bottom). To rule out that the observed silencing defects were due to instability of the mutant Tas3 proteins, we examined the levels of wild-type and mutant Tas3 protein by western blotting and found that the mutant proteins were expressed to similar levels as the wild-type protein (Figure 3C). These results, together with the structural and biochemical evidence (Figures 1 and 2), suggest that Tas3-TAM-mediated Tas3 self-association is required for RITS spreading from centromeric *otr* to *imr* repeats.

Mutant Tas3-TAM Proteins Assemble into RITS Complexes with Dramatically Reduced siRNA Levels

Tas3 bridges Ago1 and Chp1 (Partridge et al., 2007). To determine RITS complex formation in the *tas3-TAM* mutants, we performed coimmunoprecipitation experiments using TAP-tagged wild-type and mutant Tas3 proteins, including a Tas3 C-terminal truncation (Tas3ΔTAM), which removes the last 128 amino acids. We found that mutant proteins coimmunoprecipitated with Chp1 and FLAG-Ago1 with similar efficiency as the wild-type protein (Figures 4A and 4B, compare lane 1 with lanes 2−5). This result demonstrates that RITS complex formation is not affected in *tas3-TAM* mutants and that the C terminus of Tas3 is not involved in Chp1 or Ago1 binding (also shown in Partridge et al. [2007]).

Deletion of *tas3* results in the complete loss of *cen* siRNAs. To determine the effect of *tas3-TAM* mutations on *cen* siRNAs levels, we performed northern blot analysis on RNAs isolated from wild-type, *tas3Δ*, and *tas3-TAM* mutant cells. We found a dramatic reduction in the levels of both total (Figure 4C) and Ago1-purified (Figure 4D) *cen* siRNAs in all *tas3-TAM* mutants compared to wild-type. Because we observed a similar decrease in *cen* siRNA levels in total and Ago1-purified northern blots, it is unlikely that the *tas3-TAM* mutations disrupt Ago1-siRNA binding. Quantification of total or FLAG-Ago1-purified siRNAs from mutant cells

(normalized to a background RNA) revealed about a 10- to 15-fold reduction in siRNA levels compared to wild-type cells (Figures 4C and 4D). These results demonstrate a role for the Tas3-TAM domain in *cen* siRNA generation and suggest that Tas3 self-association may be required for efficient dsRNA synthesis by the RDRC complex and/or its subsequent processing by Dicer.

Localization and Spreading of RITS to Centromeric *imr* Repeats Is Abolished in *tas3-TAM* Mutants

All components of RITS, including Tas3, localize to centromeric heterochromatin. RITS contains heterochromatic siRNAs that are complementary to transcripts originating from centromeric *otr* elements and are thought to base pair with these noncoding transcripts (cenRNAs). Additionally, Clr4-mediated methylation of H3K9 creates a binding site for the chromodomain of Chp1, thus stabilizing RITS association with heterochromatin. In order to test whether RITS localization and spreading is abrogated in *tas3-TAM* mutants, we performed ChIP experiments, examining Tas3 localization at *otr1*, *imr1*, *imr1R::ura4*$^+$, and *otr1R::ura4*$^+$ loci (Figure 5A).

At the *dg* and *dh* repeats, we found a consistent 2- to 3-fold reduction in mutant Tas3 occupancy compared to wild-type (Figure 5B, compare lanes 3−6 with lane 2; and Figure 5C). Also, consistent with the *otr1R::ura4*$^+$ silencing data (Figure 3B), mutant Tas3-TAM proteins associated with the *ura4*$^+$ insert at *otr1R* less efficiently than wild-type Tas3 (Figure 5D, compare lanes 3−6 with lane 2; and Figure 5E). In contrast, mutant Tas3-TAM proteins did not localize to either *imr1* or *imr1::ura4*$^+$ (Figure 5B, compare lane 2 with lanes 3−6; and Figure 5C) compared to the wild-type protein. These results demonstrate that the C terminus of Tas3 is necessary for the association of the RITS complex with the *imr* sequences, but is only partially required for RITS association with *otr*. Furthermore, these data show that RITS spreading from native centromeric repeat sequences into *ura4*$^+$ reporter transgenes requires Tas3-TAM, suggesting that TAM-mediated Tas3 self-association is necessary for RITS spreading.

Tas3-TAM Is Not Required for the Spreading of H3K9 Methylation at Centromeres

Previous work has shown that spreading of H3K9me into centromeric transgenes (e.g., *imr1R::ura4*$^+$ and *otr1R::ura4*$^+$) requires RNAi proteins, including Tas3 (Volpe et al., 2002; Verdel et al., 2004). This is in contrast to the native centromeric sequences (e.g., *imr* or the *dg* and *dh* repeats of *otr*), where H3K9 methylation is only partially dependent on the RNAi pathway (see Figure 6). The data presented in Figure 5 show that, in the absence of Tas3-TAM, RITS spreading to *otr1R::ura4*$^+$ or *imr1R::ura4*$^+$ is reduced or completely abolished, respectively. Therefore we used ChIP to determine whether the loss of silencing and defect in RITS spreading caused by the Tas3-TAM mutations was accompanied by a loss or reduction in H3K9me spreading to the centromeric *ura4*$^+$ reporter genes. We examined H3K9me levels at the native centromeric *imr1*, *imr2−1*, *imr2−2*, *dg1*, *imr1R::ura4*$^+$, and *otr1R:: ura4*$^+$ reporter genes in *clr4Δ*, *wild-type*, *tas3ΔTAM*, and *tas3Δ* cells. Surprisingly, we found no defect in H3K9me in *tas3ΔTAM* compared to wild-type cells at native centromeric repeats (*dg1*, *imr1*, *imr2−1*, or *imr2−2*) or the *ura4*$^+$ inserts (for *imr1R::ura4*$^+$, compare lane 3 with lane 2 in Figure 6A; for *otr1R::ura4*$^+$, compare lane 5 with lane 2 in Figure 6C; note quantification is shown in Figures 6B and 6D, respectively). As a control, consistent with previous reports (Verdel et al., 2004), in *tas3Δ* cells, we observed a 3- to10-fold reduction in H3K9me levels at native *cen* and a complete loss of H3K9me at *otr1R::ura4*$^+$ or *imr1R::ura4*$^+$ (Figure 6A, compare lane 4 and lane 2; and Figure 6C, compare lane 6 and lane 2). Furthermore, as shown previously (Sadaie et al., 2004; Motamedi et al., 2008), H3K9 methylation of native centromeric sequences or *otr1R::ura4*$^+$ reporter occurred independently of Swi6 or Chp2 proteins. Thus, although Tas3-TAM was required for efficient silencing and RITS spreading (Figures 4 and 5), it was not required for H3K9 methylation. We conclude that Tas3-TAM-

mediated RITS spreading acts downstream of H3K9 methylation and probably mediates silencing through RNAi-dependent degradation of centromeric transcripts.

DISCUSSION

The data presented in this study provide insight into the mechanism of RITS spreading and its role in gene silencing at the *S. pombe* pericentromeric DNA regions. First, the structure of the C-terminal ~120 amino acids of Tas3 (Tas3-TAM) reveals an α-helical domain capable of polymeric self-association in vitro. Second, deletion of the Tas3-TAM or amino acid substitutions that abrogate its polymerization in vitro result in loss of silencing of a reporter gene inserted at centromeric *imr* repeats in vivo. Third, in *tas3-TAM* polymerization mutant cells, spreading of RITS to the centromeric *imr* repeats is abolished but H3K9 methylation levels are unaffected. Together with the dramatic reduction of siRNA accumulation in *tas3-TAM* mutant cells, our findings support an additional role for RITS in heterochromatic gene silencing that is independent of the requirement of RNAi in amplification of H3K9 methylation. The implications of these findings for the mechanism of RNAi-dependent heterochromatic gene silencing are discussed below.

Tas3-TAM Domain, an All-α-Helical Module Required for RITS *cis* Spreading

Tas3 bridges Chp1 and Ago1 within the RITS complex, thereby physically connecting an H3K9me-binding protein (Chp1) with an RNAi effector protein (Ago1). It has been shown that Tas3 interacts with Chp1 through its N-terminal domain (DeBeauchamp et al., 2008; Petrie et al., 2005) and binds to Ago1 through a “GW”-rich domain found in the middle of Tas3 (Partridge et al., 2007; Till et al., 2007). Our current work allows a further dissection of Tas3 functional domains, revealing that the C-terminal TAM domain acts as a self-association domain and facilitates RITS *cis* spreading within centromeric repeat regions (Figures 1A and 5). Consistent with the above findings, deletion of the TAM domain from Tas3 did not affect RITS complex formation (Figures 4A and 4B); however, such truncation resulted in a loss or reduction in silencing of *ura4*$^{+}$ gene inserted at the centromeric *imr* or *otr* regions, respectively (Figure 3B), indicating an important role of C-terminal Tas3-TAM domain in RITS-mediated heterochromatic gene silencing.

Structural analyses of the TAM polymer enabled us to design point mutations that specifically block polymer formation. The pronounced silencing defect of the *ura4+* gene inserted at *imr* in contrast to the weaker silencing defect at *otr* in the *tas3-TAM* point mutant cells (Figure 3B) supports a critical role of TAM-mediated Tas3-Tas3 interactions in RITS spreading from nucleation sites within *otr* to adjacent regions, like *imr* (Figure 7). It is conceivable that these interactions promote the successive binding of RITS complexes from nucleation sites to nearby sites on chromatin entropically favorable. We propose that Tas3-mediated RITS self-association works cooperatively with Chp1 binding to H3K9me and/or Ago1-loaded siRNAs base pairing with nascent transcripts, thus ensuring a specific stable RITS recruitment and spreading on chromatin. This is similar to multivalent interactions that have been proposed to stabilize the association of other chromatin-binding proteins with multiply modified histones or DNA (Ruthenburg et al., 2007).

The all-α-helical polymerization feature of Tas3-TAM is reminiscent of the sterile alpha motif (SAM) found in transcriptional repressors, such as TEL and polycomb group (PcG) proteins Ph and Scm, in which SAM represents an ~70 amino acid all-α-helical module that is capable of polymer formation in vitro (reviewed in Kim and Bowie [2003] and Qiao and Bowie [2005]). Similar to the situation with the TAM domain, which is present in a complex that mediates chromatin targeting, these SAM-containing transcriptional repressors also harbor either DNA binding modules (e.g., Ets DNA binding domain of TEL) or histone effector modules (e.g., chromodomain within the PcG complexes) for chromatin association. Likewise,

in vivo studies revealed that SAM polymer-blocking mutations in TEL (Wood et al., 2003), as well as in Scm (Peterson et al., 2004), disrupted the repressive function of their respective proteins. PcG complexes regulate facultative heterochromatin formation associated with histone H3K27me during metazoan development, and evidence in support of their connection to RNAi machineries has been reported recently (Grimaud et al., 2006; Kim et al., 2006; Liu et al., 2007). As such, the functional similarity between RITS TAM and PcG SAM suggests the existence of convergently evolved strategies shared by distantly related eukaryotes in which a polymerization module promotes silent chromatin assembly. Further support for this notion comes from the observed oligomeric self-association of Sir3 within the SIR-silencing complex in budding yeast (Liou et al., 2005).

Moreover, given the existence of a potential binding pocket in the exposed surface of the TAM polymer (Figures 1C and 1D), it is possible that TAM may exert other functions besides polymerization, for example, as a protein interaction platform to recruit other RITS interacting factors. This possibility is supported by the more severe silencing defect of *tas3ΔTAM* cells compared to the other polymer-blocking point mutants, especially for the *otr::ura4*$^{+}$ reporter gene (Figure 3B).

The requirement for both siRNAs and H3K9 methylation in localization of RITS to centromeric repeats suggests that the complex is recruited to chromatin by cooperative interactions involving its siRNA-programmed Ago1 and its chromodomain Chp1 subunits, respectively (Figure 7). However, this model does not explain how RITS spreads to sites that may not give rise to any siRNA, such as the *imr* repeat regions. The data presented in this report suggest that RITS spreading from transcribed centromeric heterochromatin nucleation centers to untranscribed regions with few or no siRNAs may be mediated by Tas3 self-association. Specifically, the point mutations within the Tas3-TAM, which disrupt Tas3 polymerization in vitro, abrogate Tas3 spreading to the native centromeric *imr1* and a *ura4*$^{+}$ transgene inserted within *imr1* (*imr1R::ura4*$^{+}$), but cause only a slight defect in RITS localization to native *otr* sequences (Figures 5 and 6). These observations suggest that Tas3-Tas3 interactions are particularly important for RITS spreading into regions with few or no siRNAs (Figure 7).

Role of siRNAs and RITS Polymerization in H3K9me Spreading

Artificial tethering of Tas3 to the transcript of a euchromatic gene leads to the RNAi-dependent silencing of the gene, consequent H3K9me, and Swi6 recruitment (Buhler et al., 2006). This demonstrates that RNAi can recruit the CLRC H3K9 methyltransferase to mediate heterochromatin assembly, providing a mechanistic basis for the RNAi-dependent spreading and amplification of H3K9 methylation within the centromeric repeat regions. Here, we found that in the absence of Tas3-TAM domain, which mediates Tas3 self-association in vitro and RITS spreading in vivo, the spreading of H3K9me to the reporter constructs (*cen::ura4*$^{+}$) is unaffected, demonstrating that CLRC-mediated H3K9 spreading can occur in the absence of RITS spreading. This observation suggests that initiation of RNAi-dependent H3K9 methylation in centromeric regions requires RITS, while the subsequent spreading of H3K9 methylation can occur in the absence of detectable RITS spreading. A possible explanation for these observations is that once a threshold level of H3K9 methylation is achieved, other mechanisms, such as a previously proposed mechanism involving the association of the chromodomain of Clr4 with H3K9me (Noma et al., 2004; Zhang et al., 2008), mediate the subsequence spreading of Clr4 and H3K9 methylation (Figure 7). Alternatively, in the absence of polymerization, RITS may mediate H3K9 methylation at the *imr* region without stably associating with chromatin, possibly by associating with nascent *imr* transcripts (Figure 7). We favor the former possibility because transcripts and siRNAs originating from *imr* or *imr*-inserted trangenes are rare or undetectable (Buhler et al., 2007).

RITS Spreading and Cotranscriptional Gene Silencing

Heterochromatic gene silencing in fission yeast results from a combination of distinct repressive mechanisms. In addition to transcriptional gene silencing, stable repression requires two different RNA-processing mechanisms involving RNAi and/or the TRAMP/exosome RNA degradation machinery (Buhler et al., 2007). The data presented in this paper demonstrate that the spreading of RITS itself is required for silencing of a reporter gene inserted at the centromeric *imr* region, independently of RITS-dependent spreading of H3K9 methylation. Because recruitment of the SHREC2 complex and histone H3K14 deacetylation, which limit RNA Pol II access to chromatin, occur downstream of H3K9 methylation (Sugiyama et al., 2007; Motamedi et al., 2008), loss of *imr1R::ura4*$^{+}$ silencing in *tas3-TAM* polymerization-defective mutant cells is likely to result from a defect in RITS-mediated RNA degradation. Consistent with this possibility, *tas3-TAM* polymerization mutants have dramatically reduced levels of centromeric siRNAs, indicating a defect in the RNAi-dependent processing of centromeric noncoding transcripts.

We have proposed previously that the physical association of RITS and RDRC is important for targeting of RDRC to heterochromatic noncoding transcripts (Motamedi et al., 2004), which is critical for Rdp1-dependent dsRNA synthesis and Dcr1-dependent siRNA generation (Colmenares et al., 2007). The dramatic reduction in siRNA levels in *tas3-TAM* mutant cells may result from a defect in the ability of RITS to facilitate RDRC template targeting. The subdomain structure of Tas3-TAM is similar to the XD domain of the measles P protein, a small subunit of the measles viral RNA polymerase (Kingston et al., 2004), raising the possibility that Tas3-TAM may be similarly involved in the recruitment of RDRC to its target transcripts. Alternatively, the decrease in RITS recruitment to transcribed centromeric *otr* regions (Figure 5B) and a concomitant decrease in RDRC/Dcr1 recruitment may be responsible for less efficient dsRNA synthesis and reduced siRNA levels.

Conclusions

Our combined structural, biochemical, and in vivo functional studies have uncovered a polymeric self-association property in Tas3, and therefore in the RITS complex, through a previously unidentified alpha motif in the Tas3 C terminus. We demonstrate that this alpha motif is required for RITS *cis* spreading, efficient siRNA generation, and heterochromatic gene silencing. Our findings suggest that Tas3-TAM-mediated RITS *cis* spreading as well as H3K9me- and siRNA-mediated RITS recruitment act cooperatively to propagate the silencing machineries along the chromatin fiber for efficient establishment and maintenance of silent chromosome domains.

EXPERIMENTAL PROCEDURES

Molecular Cloning, Protein Expression, and Purification

Recombinant Tas3 Te (426−549), Te1 (426−545), Th (380−549), and full-length (1−549) protein samples were overexpressed and purified from *E. coli*. Details of vector construction, mutagenesis, protein expression, and purification are listed in the Supplemental Experimental Procedures.

Crystallization, Data Collection, and Structure Determination

All crystals were grown by the hanging-drop vapor-diffusion method at 293 K. Diffraction data were collected at the National Synchrotron Light Source beam line X9A (currently X3A) (Brookhaven National Laboratory). Structures were determined by selenium single-wavelength anomalous dispersion (SAD) and molecular replacement methods. Detailed

crystallization conditions, data collection, and structure determination procedures are outlined in the Supplemental Experimental Procedures.

Analytical Gel-Filtration Analysis

Analytical gel-filtration analyses of Te, TeDM, Th, and Th(L479E) samples were performed on the ACTA purifier system (GE Healthcare) with the Superdex 75 10/300 GL column. The buffer system for elution is 20 mM Tris (pH 7.5) and 50 mM KCl for Te and TeDM and 20mM Tris (pH 8.5) and 100 mM KCl for Th and Th(L479E).

NMR Spectroscopy

NMR samples of ^{15}N-labeled Te and TeDM were prepared in the buffer: 50 mM KCl and 20 mM Na/K phosphate (pH 7.5). ^{1}H-^{15}N HSQC spectra were recorded at 298 K on Varian Unity 600 spectrometers and processed using NMRPipe/NMRDraw (Delaglio et al., 1995).

Biochemical Crosslinking Assays

Crosslinking assays were performed using the BS^3 crosslinker (Pierce). In general, a total of 200 μl of reaction system was prepared by mixing fresh BS^3 crosslinker and the protein samples to a final concentration of 5 mM and 4 mg/ml, respectively, in the Tris-free buffer (150 mM NaCl and 20 mM HEPESNa [pH 7.5]) at room temperature. At different time points, 20 μl of reaction mixture was transferred into a tube containing 10 μl of quench buffer (0.1 M Tris [pH 7.5]), followed by the addition of 10 μl of 4× SDS loading dye. Then the crosslinked samples were analyzed on 4%–12% NuPAGE gradient gels (Invitrogen) under denaturing conditions and stained by Coomassie blue for visualization.

Before crosslinking, protein buffers were exchanged into Tris-free solution by desalting column if necessary. Full-length Tas3 was prepared in 0.5 M NaCl and 20 mM HEPESNa (pH 8.2) for better protein stability, and a protein concentration of 1.5 mg/ml was used for the crosslinking assay. Bovine RNase A control was purchased from GE Healthcare (LMW Calibration Kit) as lyophilized powder and was prepared by weighing. Protein concentrations of all other Tas3 samples were measured based on the UV absorption at 280 nm.

Electron Microscopy

Protein samples were adsorbed to a glow-discharged copper grid overlaid with carbon-coated collodion film and negatively stained with uranyl formate as described previously (Ohi et al., 2004). Grids were inspected with a Phillips CM10 electron microscope operated at an acceleration voltage of 100 kV. Images were recorded at a magnification of 21,000 on a charge-coupled device camera.

Strain Construction

All *S. pombe* strains used in this study are listed in Table S1. Detailed procedures for strain construction are listed in the Supplemental Experimental Procedures.

Silencing Assays

All silencing assays were performed as described previously (Verdel et al., 2004). Briefly, cells were grown to logarithmic phase in yeast extract supplemented with adenine. Five-fold serial dilutions of each culture were spotted on YEA or YEA plus 5-fluoro-oratic acid plates and photographed after 2−3 days of growth at 32° C.

TCA Western

Ten milliliters of logarithmic phase cells (OD_{600} = 0.5) were frozen and resuspended in 0.5 ml of cold TCA buffer (20 mM Tris [pH 8.0], 50 mM ammonium acetate, 2 mM EDTA, 2 mM PMSF, 2 mM Leupeptin, and 2 mM aprotinin), 0.5 ml of cold 30% TCA, and 0.5 ml of cold glass beads. Cells were lysed by bead-beating the samples four times for 30 s in a BioSpec Minibead-beater-8 with 2 min of on-ice cooling in between each interval. After lysis, the supernatant was spun and the pellet was washed once with 1 ml of cold acetone. The acetone was then removed and the pellet was dissolved in 100 μl of 65 degree SDS-PAGE sample buffer for 10 min. Standard SDS-PAGE and transfer methods were used to detect the level of wild-type and mutant TAP-tagged Tas3 proteins (Motamedi et al., 2004). The monoclonal anti-actin antibody from Millipore was used as the loading control.

Immunoprecipitation Assays

In Figure 4A, the Tas3-TAP and FLAG-Ago1 coimmunoprecipitation experiments were performed exactly as described previously (Motamedi et al., 2004), except the monoclonal FLAG antibody (Sigma, F1804) was used to detect Ago1 protein. In Figure 4B, mutant and wild-type Tas3 proteins were purified as described previously (Motamedi et al., 2004), except the purified material was subjected to western analysis using anti-CBP (Open Biosystems, CAB1001) and Chp1 antibodies (Abcam, 18191) after the TEV cleavage step. Ten to fifteen grams of frozen cells were used for each of the one-step TAP purifications.

Northern Blots

All northern blots with total or Ago1-purified RNA, including the list of centromeric oligos used as probes, were done as described previously (Buhler et al., 2006, 2007).

ChIP

All Tas3-TAP ChIP experiments were performed as described previously (Huang and Moazed, 2003; Motamedi et al., 2004). Briefly, cells were grown to logarithmic phase (OD = 1.5 − 2.0) in YEA, incubated in 1% formaldehyde for 15 min, spun, and frozen in liquid nitrogen for later use. Immunoprecipitations were performed for 1−2 hr with the dimethylated H3K9 antibody (Abcam, ab1220) or protein A beads for TAP-tagged proteins. For H3K9me ChIP, Dyna-beads Protein A (Invitrogen) was used instead of protein A Sepharose beads. The linear range for PCR for each sample was determined empirically and a final radioactive PCR was performed for each sample using these conditions. PCR products were run on 6% acrylamide gels and dried and exposed to X-ray film and phosphorimager screen for quantification. Primer sequences are provided in Table S2.

Supplementary Material

Refer to Web version on PubMed Central for supplementary material.

ACKNOWLEDGMENTS

We thank Dr. Babu Manjasetty at the National Synchrotron Light Source X3A, Brookhaven National Laboratory, supported by the U.S. Department of Energy, for assistance with data collection. We also thank Lena Liang for assistance in recombinant protein purification, Xiaotian Tong and Jikui Song for NMR spectroscopy data collection, Min Lu for Circular Dichroism spectra acquisition, Shiv Grewal and Karl Ekwall for *S. pombe* strains, Tetsushi Iida and Marc Buhler for primers, and Andre Verdel for strain construction and contributions to early phases of this project. M.R.M. is supported by a postdoctoral fellowship from the Canadian Institute of Health Research and thanks Ali Motamedi for his endless sacrifices and support throughout his life. C.K.Y. is supported by a postdoctoral fellowship from the Jane Coffin Childs Memorial Fund. This work was supported by funds from the National Institutes of Health (D.M.), the Abby Rockefeller Mauze Trust (D.J.P.), and the Dewitt Wallace and Maloris Foundations (D.J.P.). D.M. and T.W. are Howard Hughes Medical Institute Investigators.

REFERENCES

Bannister AJ, Zegerman P, Partridge JF, Miska EA, Thomas JO, Allshire RC, Kouzarides T. Selective recognition of methylated lysine 9 on histone H3 by the HP1 chromo domain. Nature 2001;410:120–124. [PubMed: 11242054]

Buhler M, Verdel A, Moazed D. Tethering RITS to a nascent transcript initiates RNAi- and heterochromatin-dependent gene silencing. Cell 2006;125:873–886. [PubMed: 16751098]

Buhler M, Haas W, Gygi SP, Moazed D. RNAi-dependent and -independent RNA turnover mechanisms contribute to heterochromatic gene silencing. Cell 2007;129:707–721. [PubMed: 17512405]

Buhler M, Spies N, Bartel D, Moazed D. TRAMP-mediated RNA surveillance prevents spurious entry of RNAs into the *Schizosaccharomyces pombe* siRNA pathway. Nat. Struct. Mol. Biol 2008;15:1015–1023. [PubMed: 18776903]

Cam HP, Sugiyama T, Chen ES, Chen X, FitzGerald PC, Grewal SI. Comprehensive analysis of heterochromatin- and RNAi-mediated epigenetic control of the fission yeast genome. Nat. Genet 2005;37:809–819. [PubMed: 15976807]

Colmenares SU, Buker SM, Buhler M, Dlakic M, Moazed D. Coupling of double-stranded RNA synthesis and siRNA generation in fission yeast RNAi. Mol. Cell 2007;27:449–461. [PubMed: 17658285]

DeBeauchamp JL, Moses A, Noffsinger VJ, Ulrich DL, Job G, Kosinski AM, Partridge JF. Chp1-Tas3 interaction is required to recruit RITS to fission yeast centromeres and for maintenance of centromeric heterochromatin. Mol. Cell. Biol 2008;28:2154–2166. [PubMed: 18212052]

Delaglio F, Grzesiek S, Vuister GW, Zhu G, Pfeifer J, Bax A. Nmrpipe—A Multidimensional Spectral Processing System Based on Unix Pipes. J. Biomol. NMR 1995;6:277–293. [PubMed: 8520220]

Djupedal I, Portoso M, Spahr H, Bonilla C, Gustafsson CM, Allshire RC, Ekwall K. RNA Pol II subunit Rpb7 promotes centromeric transcription and RNAi-directed chromatin silencing. Genes Dev 2005;19:2301–2306. [PubMed: 16204182]

Ekwall K. The roles of histone modifications and small RNA in centromere function. Chromosome Res 2004;12:535–542. [PubMed: 15289661]

Gaboriaud C, Bissery V, Benchetrit T, Mornon JP. Hydrophobic cluster analysis: an efficient new way to compare and analyse amino acid sequences. FEBS Lett 1987;224:149–155. [PubMed: 3678489]

Grewal SIS, Moazed D. Heterochromatin and epigenetic control of gene expression. Science 2003;301:798–802. [PubMed: 12907790]

Grimaud C, Bantignies F, Pal-Bhadra M, Ghana P, Bhadra U, Cavalli G. RNAi components are required for nuclear clustering of Polycomb group response elements. Cell 2006;124:957–971. [PubMed: 16530043]

Huang J, Moazed D. Association of the RENT complex with nontranscribed and coding regions of rDNA and a regional requirement for the replication fork block protein Fob1 in rDNA silencing. Genes Dev 2003;17:2162–2176. [PubMed: 12923057]

Jacobs SA, Taverna SD, Zhang YN, Briggs SD, Li JM, Eissenberg JC, Allis CD, Khorasanizadeh S. Specificity of the HP1 chromo domain for the methylated N-terminus of histone H3. EMBO J 2001;20:5232–5241. [PubMed: 11566886]

Kim CA, Bowie JU. SAM domains: uniform structure, diversity of function. Trends Biochem. Sci 2003;28:625–628. [PubMed: 14659692]

Kim DH, Villeneuve LM, Morris KV, Rossi JJ. Argonaute-1 directs siRNA-mediated transcriptional gene silencing in human cells. Nat. Struct. Mol. Biol 2006;13:793–797. [PubMed: 16936726]

Kingston RL, Hamel DJ, Gay LS, Dahlquist FW, Matthews BW. Structural basis for the attachment of a paramyxoviral polymerase to its template. Proc. Natl. Acad. Sci. USA 2004;101:8301–8306. [PubMed: 15159535]

Krissinel E, Henrick K. Secondary-structure matching (SSM), a new tool for fast protein structure alignment in three dimensions. Acta Crystallogr. D Biol. Crystallogr 2004;60:2256–2268. [PubMed: 15572779]

Lachner M, O'Carroll N, Rea S, Mechtler K, Jenuwein T. Methylation of histone H3 lysine 9 creates a binding site for HP1 proteins. Nature 2001;410:116–120. [PubMed: 11242053]

Liou GG, Tanny JC, Kruger RG, Walz T, Moazed D. Assembly of the SIR complex and its regulation by O-acetyl-ADP-ribose, a product of NAD-dependent histone deacetylation. Cell 2005;121:515–527. [PubMed: 15907466]

Liu Y, Taverna SD, Muratore TL, Shabanowitz J, Hunt DF, Allis CD. RNAi-dependent H3K27 methylation is required for heterochromatin formation and DNA elimination in *Tetrahymena*. Genes Dev 2007;21:1530–1545. [PubMed: 17575054]

Motamedi MR, Verdel A, Colmenares SU, Gerber SA, Gygi SP, Moazed D. Two RNAi complexes, RITS and RDRC, physically interact and localize to noncoding centromeric RNAs. Cell 2004;119:789–802. [PubMed: 15607976]

Motamedi MR, Hong EJ, Li X, Gerber S, Denison C, Gygi S, Moazed D. HP1 proteins form distinct complexes and mediate heterochromatic gene silencing by nonoverelapping mechanisms. Mol. Cell 2008;32:778–790. [PubMed: 19111658]

Nakayama J, Rice JC, Strahl BD, Allis CD, Grewal SIS. Role of histone H3 lysine 9 methylation in epigenetic control of heterochromatin assembly. Science 2001;292:110–113. [PubMed: 11283354]

Nicholls A, Sharp KA, Honig B. Protein folding and association: insights from the interfacial and thermodynamic properties of hydrocarbons. Proteins Struct. Funct. Genet 1991;11:281–296. [PubMed: 1758883]

Noma K, Sugiyama T, Cam H, Verdel A, Zofall M, Jia S, Moazed D, Grewal SI. RITS acts in cis to promote RNA interference-mediated transcriptional and post-transcriptional silencing. Nat. Genet 2004;36:1174–1180. [PubMed: 15475954]

Ohi M, Li Y, Cheng Y, Walz T. Negative staining and image classification—powerful tools in modern electron microscopy. Biol. Proced. Online 2004;6:23–34. [PubMed: 15103397]

Partridge JF, Scott KSC, Bannister AJ, Kouzarides T, Allshire RC. cis-acting DNA from fission yeast centromeres mediates histone H3 methylation and recruitment of silencing factors and cohesin to an ectopic site. Curr. Biol 2002;12:1652–1660. [PubMed: 12361567]

Partridge JF, DeBeauchamp JL, Kosinski AM, Ulrich DL, Hadler MJ, Noffsinger VJ. Functional separation of the requirements for establishment and maintenance of centromeric heterochromatin. Mol. Cell 2007;26:593–602. [PubMed: 17531816]

Peterson AJ, Mallin DR, Francis NJ, Ketel CS, Stamm J, Voeller RK, Kingston RE, Simon JA. Requirement for sex comb on midleg protein interactions in *Drosophila* polycomb group repression. Genetics 2004;167:1225–1239. [PubMed: 15280237]

Petrie VJ, Wuitschick JD, Givens CD, Kosinski AM, Partridge JF. RNA interference (RNAi)-dependent and RNAi-independent association of the Chp1 chromodomain protein with distinct heterochromatic loci in fission yeast. Mol. Cell. Biol 2005;25:2331–2346. [PubMed: 15743828]

Qiao F, Bowie JU. The many faces of SAM. Sci. STKE 2005;2005:re7. [PubMed: 15928333]

Rea S, Eisenhaber F, O'Carroll N, Strahl BD, Sun ZW, Schmid M, Opravil S, Mechtler K, Ponting CP, Allis CD, Jenuwein T. Regulation of chromatin structure by site-specific histone H3 methyltransferases. Nature 2000;406:593–599. [PubMed: 10949293]

Reinhart BJ, Bartel DP. Small RNAs correspond to centromere heterochromatic repeats. Science 2002;297:1831. [PubMed: 12193644]

Richards EJ, Elgin SCR. Epigenetic codes for heterochromatin formation and silencing: rounding up the usual suspects. Cell 2002;108:489–500. [PubMed: 11909520]

Ruthenburg AJ, Li H, Patel DJ, Allis CD. Multivalent engagement of chromatin modifications by linked binding modules. Nat. Rev. Mol. Cell Biol 2007;8:983–994. [PubMed: 18037899]

Sadaie M, Iida T, Urano T, Nakayama J. A chromodomain protein, Chp1, is required for the establishment of heterochromatin in fission yeast. EMBO J 2004;23:3825–3835. [PubMed: 15372076]

Scott KC, Merrett SL, Willard HF. A heterochromatin barrier partitions the fission yeast centromere into discrete chromatin domains. Curr. Biol 2006;16:119–129. [PubMed: 16431364]

Sugiyama T, Cam HP, Sugiyama R, Noma K, Zofall M, Kobayashi R, Grewal SIS. SHREC, an effector complex for heterochromatic transcriptional silencing. Cell 2007;128:491–504. [PubMed: 17289569]

Till S, Lejeune E, Thermann R, Bortfeld M, Hothorn M, Enderle D, Heinrich C, Hentze MW, Ladurner AG. A conserved motif in Argonaute-interacting proteins mediates functional interactions through the Argonaute PIWI domain. Nat. Struct. Mol. Biol 2007;14:897–903. [PubMed: 17891150]

Verdel A, Jia S, Gerber S, Sugiyama T, Gygi S, Grewal SI, Moazed D. RNAi-mediated targeting of heterochromatin by the RITS complex. Science 2004;303:672–676. [PubMed: 14704433]

Volpe TA, Kidner C, Hall IM, Teng G, Grewal SI, Martienssen RA. Regulation of heterochromatic silencing and histone H3 lysine-9 methylation by RNAi. Science 2002;297:1833–1837. [PubMed: 12193640]

White SA, Allshire RC. RNAi-mediated chromatin silencing in fission yeast. Curr. Top. Microbiol. Immunol 2008;320:157–183. [PubMed: 18268844]

Wood LD, Irvin BJ, Nucifora G, Luce KS, Hiebert SW. Small ubiquitin-like modifier conjugation regulates nuclear export of TEL, a putative tumor suppressor. Proc. Natl. Acad. Sci. USA 2003;100:3257–3262. [PubMed: 12626745]

Zhang K, Mosch K, Fischle W, Grewal SIS. Roles of the Clr4 methyltransferase complex in nucleation, spreading and maintenance of heterochromatin. Nat. Struct. Mol. Biol 2008;15:381–388. [PubMed: 18345014]

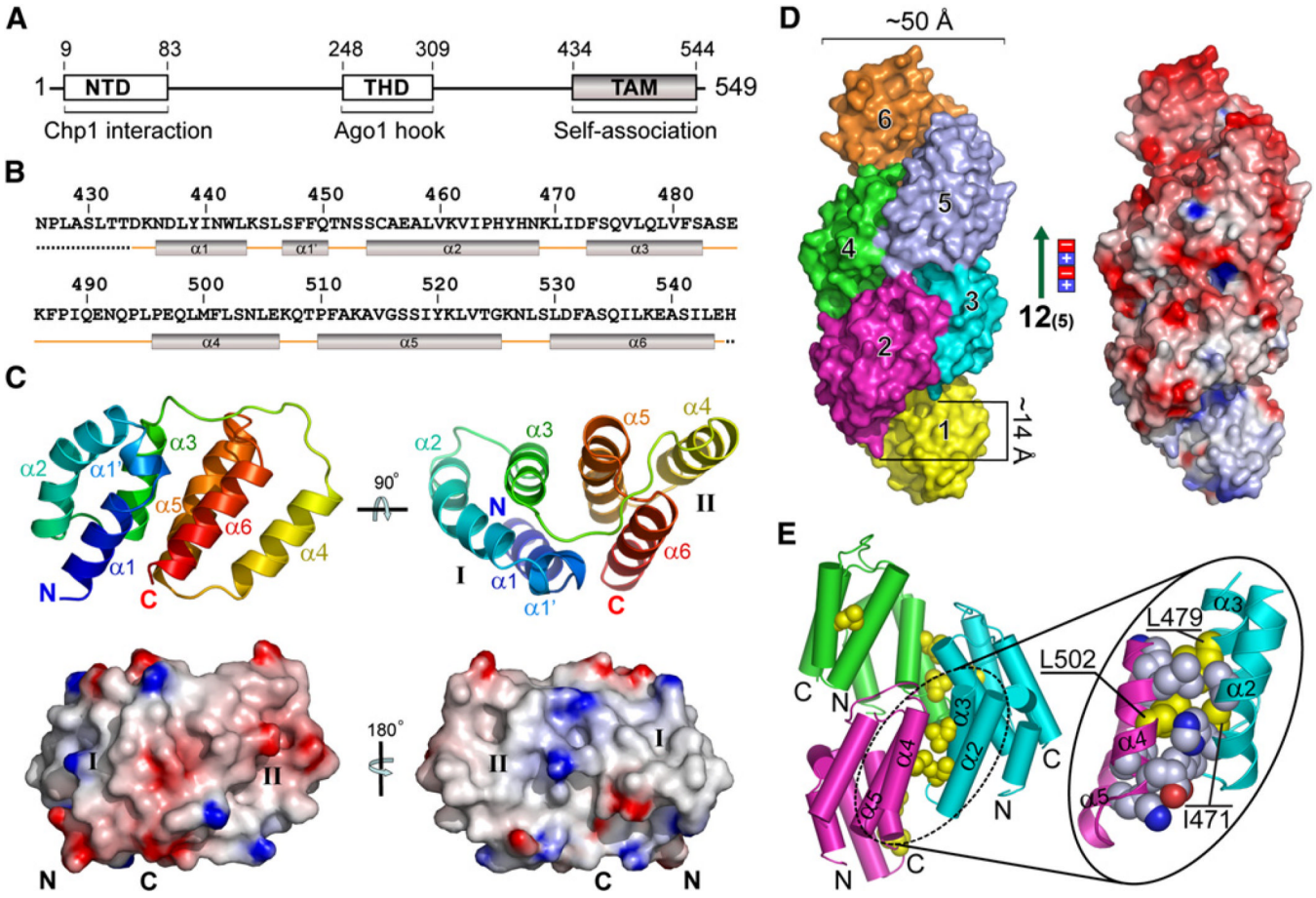

Figure 1. Structure of Tas3 C-Terminal TAM Domain and Its Self-Associated Polymer

(A) Domain architecture of full-length Tas3. The N-terminal domain (NTD) and the Tas3-homology domain (THD) are responsible for Chp1 and Ago1 interaction, respectively. The self-association C-terminal Tas3 α-helical motif (TAM) described in this paper is highlighted in gradient gray.

(B) Secondary structure alignment of the TAM-containing Te1 construct (426−545) used for the crystallographic study. Dotted line denotes the unmodeled parts of Te1 in the solved crystal structure due to their high flexibility.

(C) Ribbon and surface representations of the TAM monomer. The ribbon (top) is colored in ramp from blue (N terminus) to red (C terminus), and the surface (bottom) is colored by its electrostatic potential distribution ranging from −10 kT (red) to +10 kT (blue) as calculated by the program GRASP (Nicholls et al., 1991). The first subdomain (α1–α3) and the second subdomain (α4–α6) are denoted as I and II. The ribbon and surface drawings on the left are of the same orientation, with the bottom left and bottom right panels representing the largely exposed and buried surfaces upon self-association, respectively.

(D) Surface view of the TAM polymer. The polymer obeys approximately 12_5 screw symmetry with a diameter of ~50 Å and a rise of ~14 Å per monomer. For clarity, only half cycle of the polymer is displayed. The right panel shows the electrostatic potential distribution along the polymer with the same coloring strategy as described for (C). Note the dipole feature of the polymer with negative charges and positive charges enriched on the top and at the bottom, respectively.

(E) Details of the major polymerization interface. Key interface residue side chains are depicted in CPK with nitrogen atoms colored in blue, oxygen in red, and carbon in gray or yellow. Three

critical hydrophobic residues (I471, L479, and L502) that are used for mutagenesis study are highlighted in yellow.

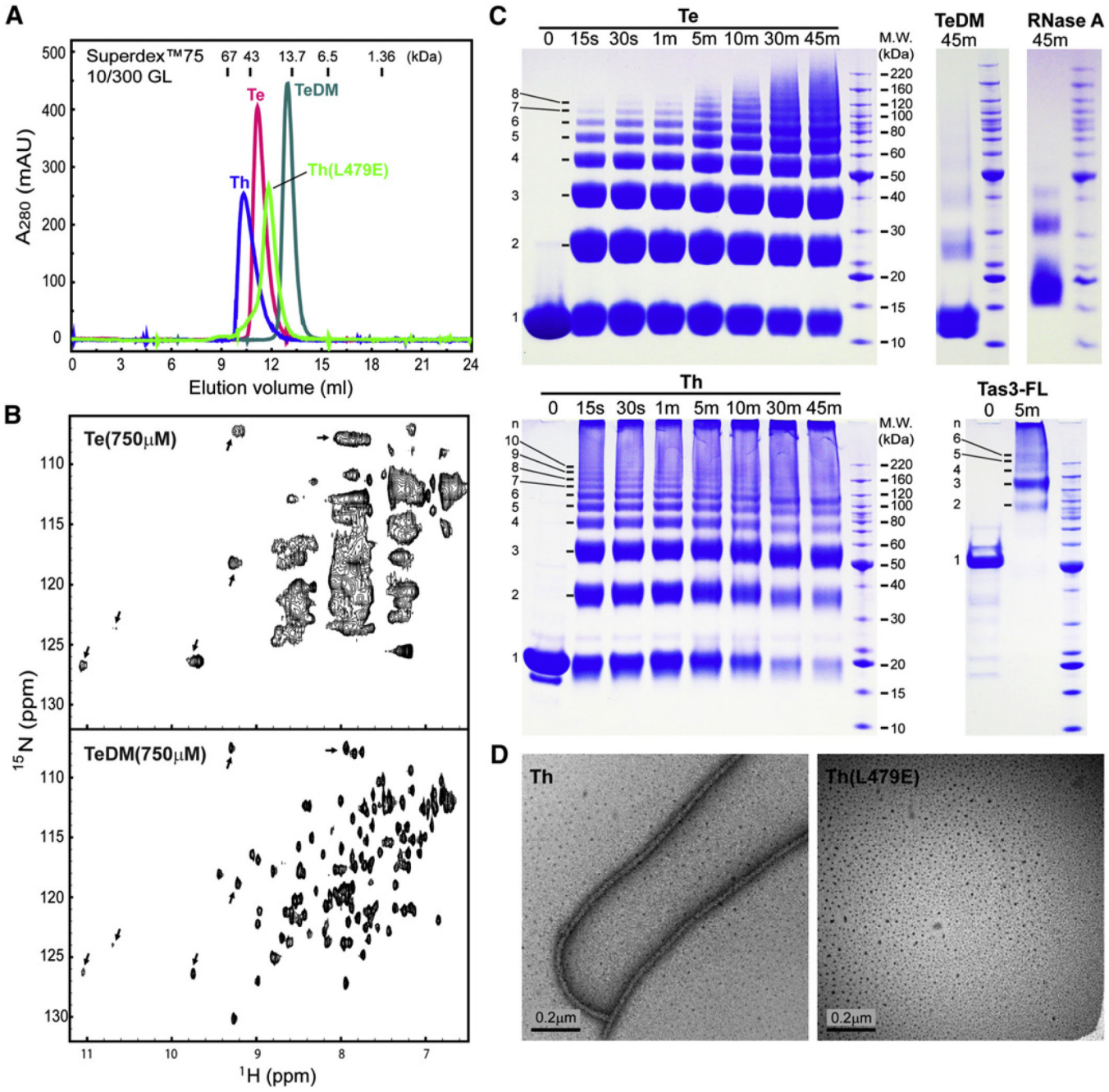

Figure 2. Tas3-TAM Domain Self-Associates in Solution

(A) Analytical gel filtration profile of wild-type Te (426−549), Te L479E/L502E double mutant (TeDM), wild-type Th (380−549), and Th L479E single mutant.

(B) ^{1}H-^{15}N-HSQC NMR spectroscopy of ^{15}N-labeled Te and TeDM samples at 750 μM; characteristic cross peaks that have similar chemical shifts in both samples are highlighted by block arrows.

(C) In vitro crosslinking assays of Te, TeDM, RNase A control, Th, and full-length Tas3 (Tas3-FL). Crosslinking was performed at a protein concentration of 1.5 mg/ml for Tas3-FL and 4 mg/ml for all other samples using amine-reactive BS^3 crosslinker. Detailed conditions are

outlined in the Experimental Procedures. Bovine RNase A was selected as a monomeric protein control due to its similar lysine composition and molecular weight compared to Te.
(D) Negative-stain electron micrograph of Th and Th(L479E).

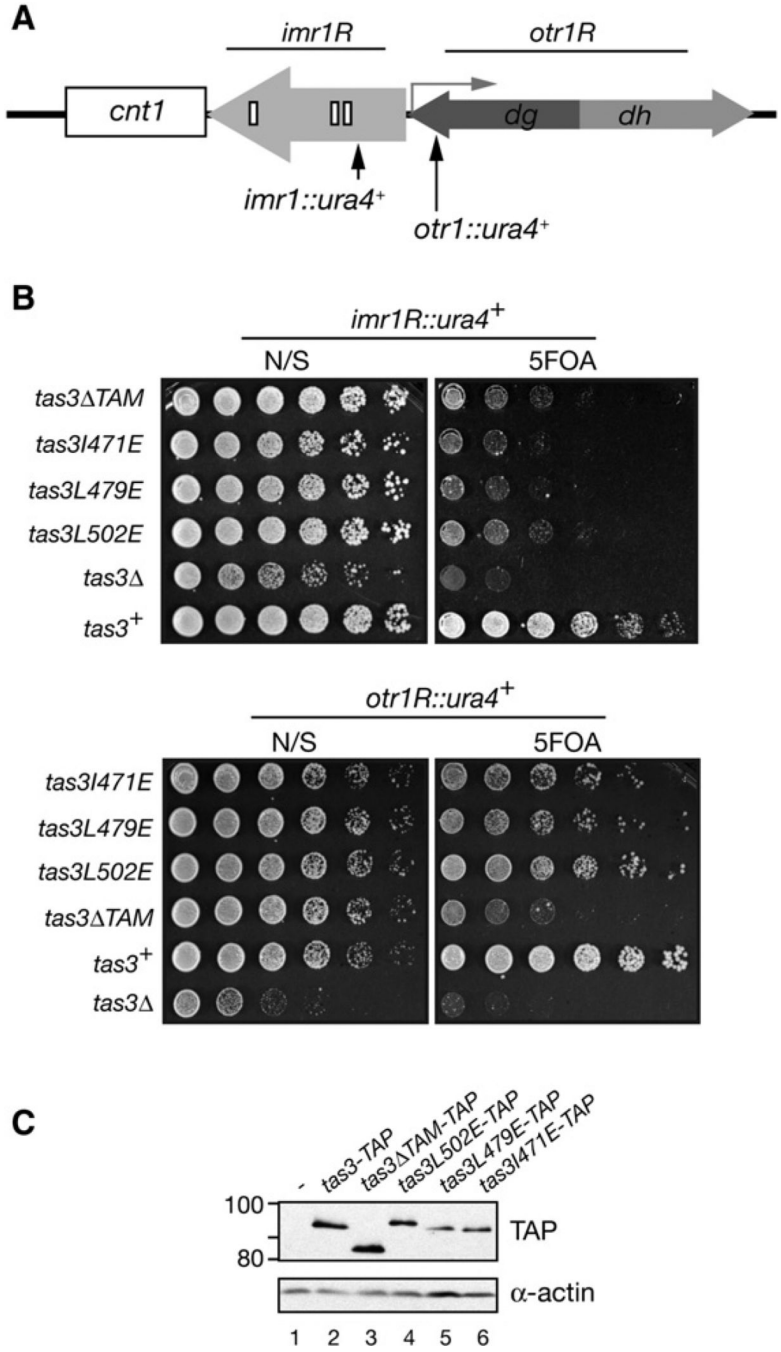

Figure 3. *tas3-TAM* Mutations Cause a Dramatic Loss of *ura4*$^+$ Silencing at *imr1* but Only a Modest Loss at *otr1*

(A) Schematic diagram of *S. pombe* centromere (*cen*) 1. The locations of *ura4*$^+$ inserts in *imr1R* and *otr1R* are shown with vertical arrows. *cnt1*, central core; *imr1*, *innermost repeat 1*; *otr1*, *outer repeat 1*; *dg* and *dh*, repeat elements in *otr*; white boxes in *imr1R*, tRNA genes.

(B) Silencing assays showing that *tas3-TAM* mutations cause a dramatic loss of *ura4*$^+$ silencing at *imr1R*, but not at *otr1R*. Note that *tas3Δ* cells have a more dramatic growth defect than *tas3-TAM* mutations. This is more apparent in the bottom panel, showing growth on N/S medium, in which the plate was photographed after a shorter period of growth.

(C) TCA western blot showing that the level of mutant Tas3 protein is similar to wild-type.

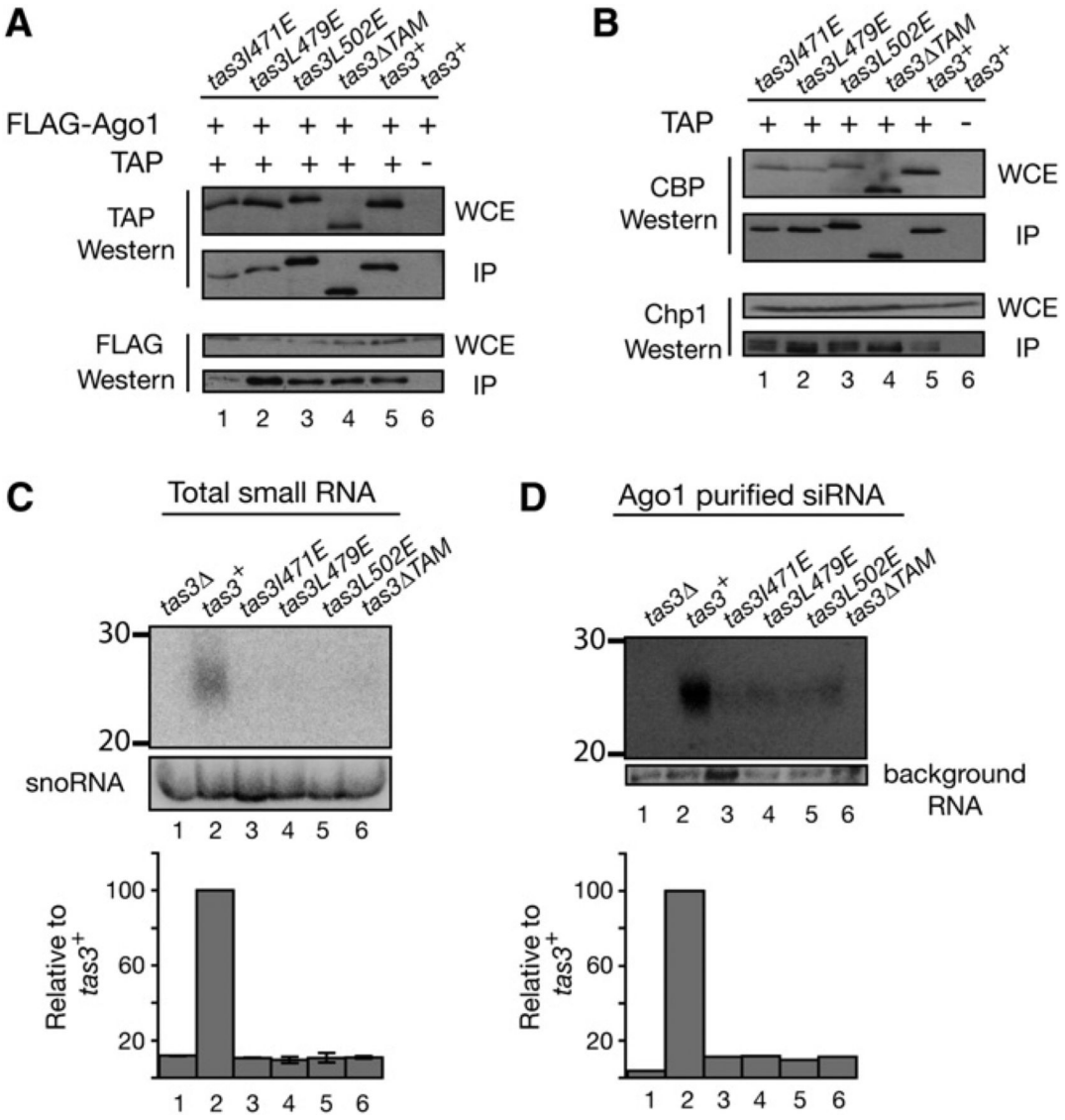

Figure 4. Mutant *Tas3-TAM* Proteins Incorporate into RITS but Cause a Dramatic Reduction in *cen* siRNA Levels

(A and B) Western blots showing that Tas3-TAP coprecipitates with FLAG-Ago1 (A) or Chp1 (B).

(C and D) End-labeled DNA oligos complementary to cen siRNAs (Verdel et al., 2004; Reinhart and Bartel, 2002) were used to probe 25 μg of total RNA (C) or 1 μg of FLAG-Ago1-associated RNA (D) from the indicated strains. snoR69 and a background RNA were used to normalize the abundance of total siRNAs (C) and Ago1-associated siRNAs (D) relative to wild-type, respectively.

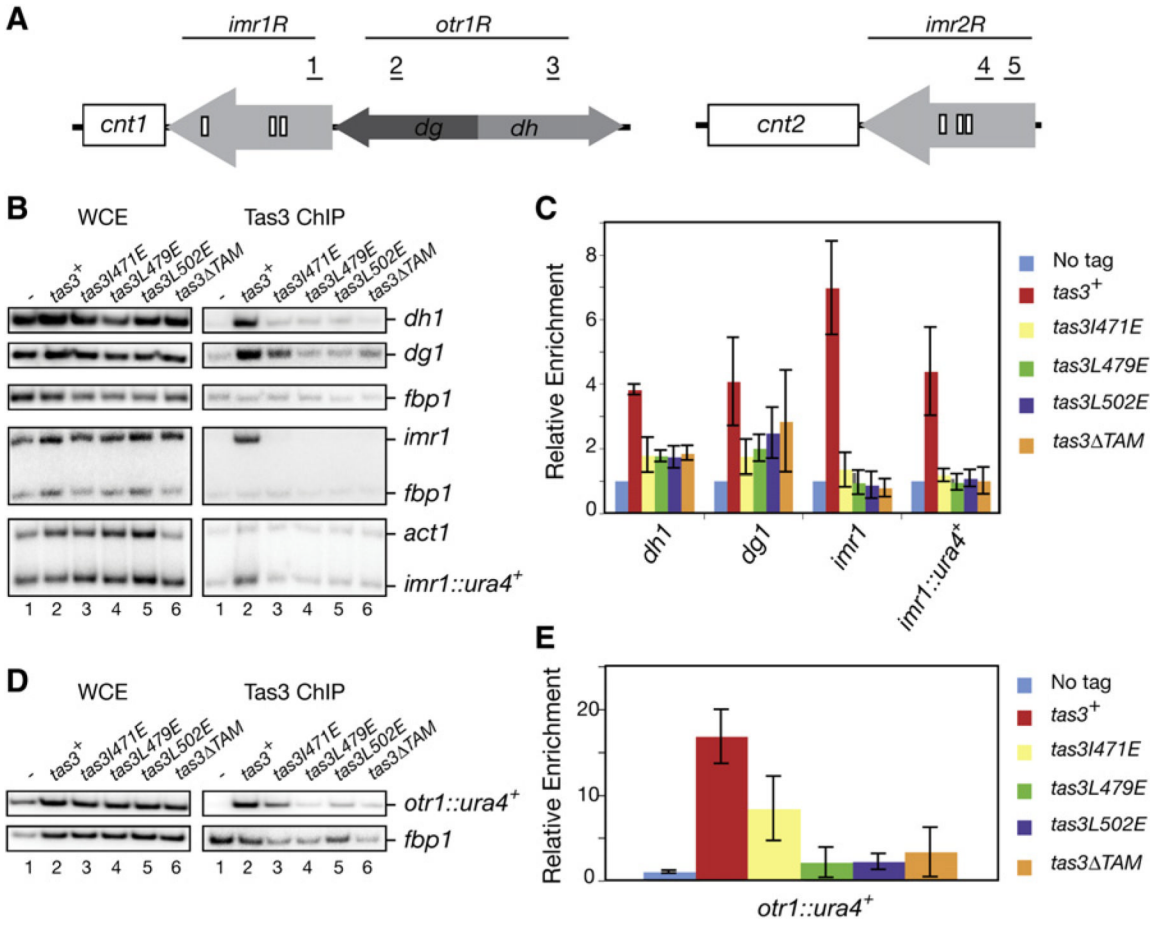

Figure 5. Tas3-TAM Domain Is Required for RITS Spreading

(A) Schematic diagram showing the location of primers in *imr1*, *dg1*, *dh1*, *imr2−1*, and *imr2−2* used in ChIP experiments. Abbreviations are described in the legend to Figure 3A.

(B–E) ChIP experiments showing Tas3-TAP localization to *imr1R* or *imr1R::ura4*$^+$ is abolished in *tas3-TAM* mutants. In contrast, a minor (2- to 3-fold; see bar graphs) decrease in Tas3-TAP occupancy at *dh1*, *dg1*, and *otr1R::ura4*$^+$ is detected in the *tas3-TAM* mutants compared to wild-type. Fold enrichment from three independent immunoprecipitations were used to generate the bar graphs (C and E). Error bars represent standard deviations. Enrichment was normalized to *act1* (for *imr1R::ura4*$^+$) or *fbp1* (for *imr1*, *dg1*, *dh1*, and *otr1R::ura4*$^+$) controls. Value for the "No tag" control was set to 1.0.

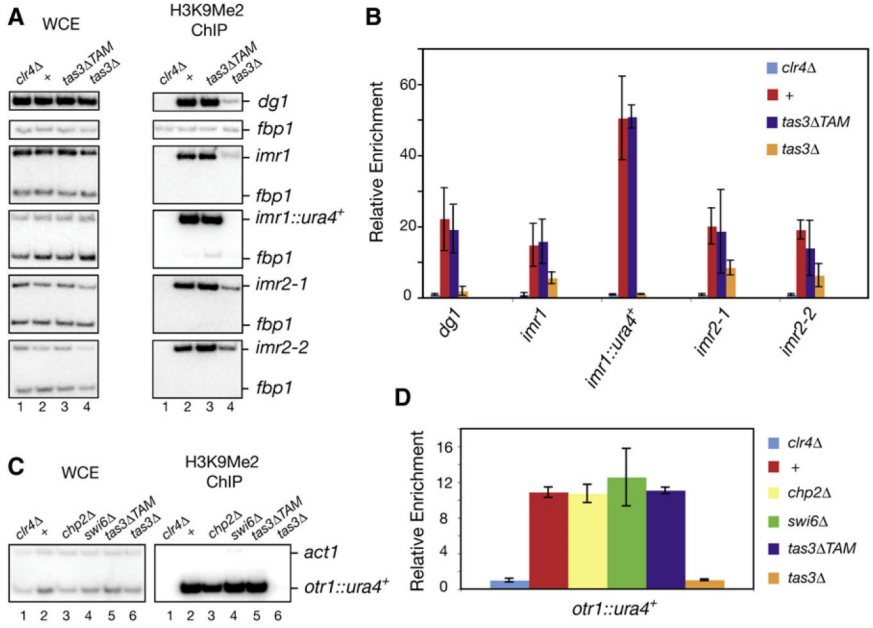

Figure 6. Tas3-TAM Is Not Required for H3K9me Spreading

(A) H3K9me ChIP experiments were performed in wild-type or mutant (*clr4Δ*, *tas3-TAM*, or *tas3Δ*) cells, and primers corresponding to pericentromeric *otr* (*dg1*), *imr* (*imr1*, *imr2−1*, and *imr2−2*), and the *imr1R::ura4*$^+$ insert were used to assess H3K9me enrichment compared to *clr4Δ* cells. The location of primers is shown in Figure 5A.

(B) Graph showing the average H3K9me levels and deviation from the mean from two independent experiments.

(C) H3K9me ChIP experiments for the *otr1-R::ura4*$^+$ transgene were performed in wild-type or mutant (*clr4Δ*, *tas3-TAM*, *chp2Δ*, *swi6Δ*, or *tas3Δ*) cells.

(D) Fold enrichment and deviation from the mean values from two independent experiments were used to generate the graphs. Enrichment was normalized to *fbp1*$^+$. Values for the *clr4Δ* control was set to 1.0.

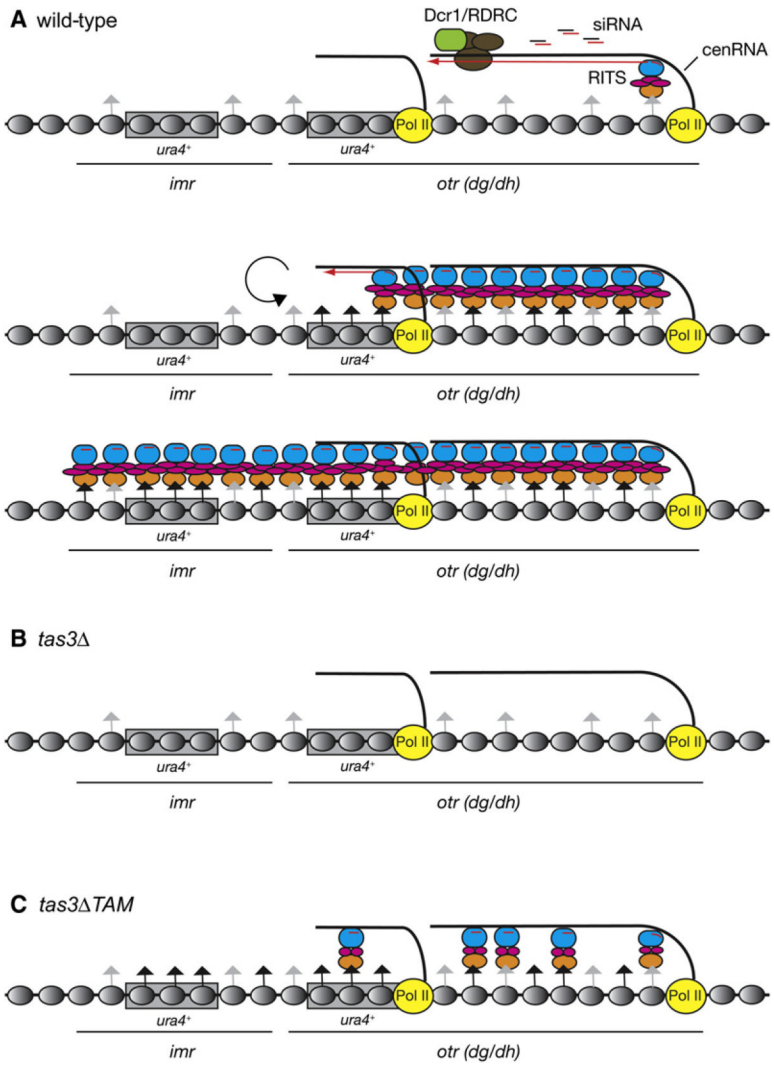

Figure 7. Model for Tas3-Mediated RITS Spreading at *S. pombe* Centromeres

(A) In wild-type cells, RITS recruitment to the centromeric *otr* region is mediated via siRNA base-pairing interactions with complementary nascent *cen* transcripts (cenRNA) and Chp1 binding to H3K9me (gray arrows). RITS recruitment targets Dcr1/RDRC to its substrate and leads to dsRNA synthesis and siRNA generation across the transcribed region. siRNA-programmed RITS mediates additional H3K9me within the *otr* region, whereas Tas3 self-association promotes the spreading of RITS and H3K9me (black arrows) across *imr* and *ura4*$^+$ reporter transgenes (rectangles). The Chp1, Tas3, and Ago1 subunits of RITS are presented in orange, magenta, and blue colors, respectively. Gray ovals, nucleosomes; yellow circles, RNA polymerase II (Pol II).

(B) In *tas3Δ* cells, RNAi-independent H3K9me is still present across *imr* and *otr* regions, but is absent from *ura4*$^+$ reporter transgenes due to the absence of siRNA-mediated spreading. (C) In *tas3ΔTAM* cells, RITS is recruited to *otr* via Ago1 siRNAs and H3K9me binding to Chp1 chromodomain, but its spreading to the *imr* region is impaired. Even though H3K9me at *imr* and *ura4*$^+$ inserted at *imr* is unaffected, RITS spreading is required for efficient silencing of the *ura4*$^+$ transgene. Reduced levels of centromeric siRNAs in *tas3ΔTAM* cells may result from a defect in Dcr1/RDRC recruitment.

Table 1

Summary of Crystallographic Analysis

Crystal	**Crystal Form I (Tetragonal)**		**Crystal Form II (Hexagonal)**
Data Collection	**Se-SAD**	**Native**	**Native**
Wavelength (Å)	0.9791	0.9772	0.9791
Space group	$P4_12_12$	$P4_12_12$	$P6_5$
Unit cell: a, b, c (Å)	64.8, 64.8, 169.5	65.0, 65.0, 169.5	84. 9, 84.9, 165.7
Resolution (Å)	20−2.4 (2.49−2.40)[a]	20−1.7 (1.76−1.70)	20−2.6 (2.69−2.60)
Unique reflections	14,928	39,086	19,969
R_{sym} (%)[b]	7.4 (30.7)	7.6 (60.8)	10.9 (65.0)
I/σ (I)	31.1 (7.5)	39.3 (4.1)	21.8 (2.6)
Completeness (%)	94.3 (95.2)	99.9 (99.9)	96.3 (90.0)
Redundancy	8.9 (8.9)	15.8 (16.0)	12.2 (12.0)
Phasing and Refinement (F > 0)			
No. of molecules per ASU	3	3	6
Solvent content	0.38	0.38	0.45
FOM after SAD and DM	0.75		
R_{work}/R_{free} (%)[c]	28.4/30.8	20.7/23.7	20.6/27.5
No. of non-H atoms			
Protein/water		2617/394	5232/176
Average B factors (Å^2)			
Protein/water		24.2/40.6	49.0/39.4
RMSD bonds			
length (Å)/angles(°)		0.005/1.13	0.007/1.24
Ramachandran plot (non-G,P)			
Most favored (%)		94.4	91.9
Additional allowed (%)		5.3	7.3
Generously allowed (%)		0.3	0.8

[a] Numbers in parentheses refer to the highest-resolution shells.

[b] $R_{sym} = \Sigma_h\Sigma_i | I_i(h) - < I(h) > | / \Sigma_h\Sigma_i I_i(h)$, where $I_i(h)$ is the *i*th measurement of reflection h, and $< I(h) >$ is the weighted mean of all measurements of h.

[c] $R = \Sigma_h||F_{obs}| - |F_{cal}|| / \Sigma_h|F_{obs}|$, where F_{obs} and F_{cal} are the observed and calculated structure factor, respectively. R_{work} and R_{free} were calculated by using the working and test set reflections, respectively.